Solar Energy Materials & Solar Cells 109 (2013) 142–147

Contents lists available at SciVerse ScienceDirect

Solar Energy Materials & Solar Cells

journal homepage: www.elsevier.com/locate/solmat

Transparent conductive film with printable embedded patterns for organic solar cells

Jong-Su Yu [a,b], Gwan Ho Jung [c], Jeongdai Jo [a], Jung Su Kim [a], Jun Woo Kim [a], Sun-Woo Kwak [a], Jong-Lam Lee [c], Inyoung Kim [a,*], Dojin Kim [b,*]

[a] Department of Printed Electronics, Korea Institute of Machinery and Materials, Daejeon 305-343, Republic of Korea
[b] Department of Materials Science and Engineering, Chungnam National University, Daejeon 305-764, Republic of Korea
[c] Department of Materials Science and Engineering, Pohang University of Science and Technology, Pohang, Gyeongbuk 790-784, Republic of Korea

ARTICLE INFO

Article history:
Received 1 August 2012
Received in revised form
9 October 2012
Accepted 10 October 2012
Available online 22 November 2012

Keywords:
Embedded Ag grid mesh
Nano-silver paste
Organic solar cells
Roll-to-roll imprint
Transparent conductive film

ABSTRACT

We report a development of a highly transparent conductive film (TCF) which is the first embedded metal grid of fine lines on a flexible substrate. The TCF reveals excellent electrical and optical performance as transparent conductive film with an extremely high σ_{DC}/σ_{OP} value of 237 due to 80.35% transmittance and 6.85 Ω/□ sheet resistance. Furthermore, the extremely high performance is realized with new features of the TCFs: roll-to-roll printability on flexible substrates, thermal imprinting of channels at 10 μm widths, water-based nano-silver paste to fill the narrow channels, and doctor blade as a facile method to fill the paste into the channels. The TCF electrode is implemented to fabrication of an organic solar cell (OSC) which shows a power conversion efficiency of 1.40%. This is non-optimized yet but approaching that of an ITO-based OSC (1.70%). Thus, we demonstrate a printable TCF to replace the ITO films toward low-cost large area roll-to-roll fabrication of organic solar cells.

1. Introduction

Indium tin oxide (ITO) is the conductor material of choice for transparent electrodes due to its high optoelectronic performance. However, two factors have recently combined to encourage the development of alternative materials and structures: the increasing cost of ITO caused by the scarcity of indium and a lack of mechanical flexibility [1]. The advent of organic solar cells (OSC) and flexible display technology requires flexibility for electrodes while maintaining high transparency and conductivity. Various transparent conductive films (TCFs) made of conducting polymers, networks of metallic nanoparticles and nanowires, carbon nanotubes and graphenes, and their composites, etc., [1,2–8] have recently been investigated, but the performance was inferior to that of ITO. Furthermore, coating technologies using relevant pastes for large-area applications has not matured. Large-area processability is indeed a practical requirement for such cost-sensitive applications, and a roll-to-roll printing technique would definitely be the first choice.

Patterned metal grids may be a promising candidate for high-performance TCFs that would be applicable to the roll-to-roll processing of large-area flexible substrates [9–11]. When applying the metal grids to OSCs as electrodes, the printing on planar substrates produces rather thin grid lines, which requires a relatively wide line width to lower the resistance of electrodes. A typical line width is on the order of 100 μm [12]. The accompanying high shadowing losses then leads to a lowering of the cell efficiency. Therefore, narrower (and thicker) metal lines can enhance the solar energy absorption by reducing the shadowing losses. The achievable line width determines the applicability to printing technology, and this depends on the size of the drawing pen and the size of the solid particles in the paste. The height of the printed line also is determined by the physical properties of the paste, which includes viscosity and solid content. Note that the steps of the printed grid lines are usually high enough to prevent a smooth over-coating by subsequent organic layers, which can cause non-uniformity of the cell performance over the cell area and bring about reliability issues. Therefore, planarization of TCF by embedding the metal grid lines into the substrate can accomplish the following: (1) it can improve the topology of the devices built upon the TCFs; and, (2) it can control the height-to-width ratio of the metal grid lines. Both effects, when applied to OSC fabrication, can ultimately enhance the cell efficiency. However, embedding metal grids into a flexible substrate requires two prerequisites: (1) a method to pattern channels of small widths (maybe less than 10 μm); and, (2) a paste (or ink) that can smoothly fill the channel via a suitable methodology. The chosen technique should be more tractable than the embedding done by

* Corresponding author. Fax: +82 42 821 7648.
E-mail address: dojin@cnu.ac.kr (D. Kim).

0927-0248/$ - see front matter © 2012 Elsevier B.V. All rights reserved.
http://dx.doi.org/10.1016/j.solmat.2012.10.013

Galagan et al. [11], and should be connected to a roll-to-roll process for large-area application. Here, we report the development of a highly transparent and conductive electrode made of embedded metal grids on a flexible substrate of polyethylene naphthalate (PEN) film. The features of the TCF are as follows: (1) it is roll-to-roll printable on a flexible substrate; (2) it allows the thermal imprinting of channels at 10 μm widths; (3) it is a water-based nano-silver paste; and, (4) doctor blading can be used to fill the paste into the channels.

2. Experimental

2.1. Fabrication of printable embedded type TCF

A schematic of the TCF fabrication process is shown in Fig. 1. The roll-to-roll processability is a key aspect of a cost-effective manufacturing method, and, therefore, all employed component technologies should be compatible with the roll-to-roll process. Thermal imprinting or hot embossing is normally conducted just above the glass transition temperature (T_g) of a polymer material [13], and a batch-type process is traditional. However, we designed a thermal imprinter made of a flexible Ni stamp for application to roll-to-roll processing. We accomplished imprinting channels with a width of 10 μm in the polymer film using the stamp.

To fill the narrow channel grids with conductive paste, an appropriate ink or paste was necessary. Conventional inks that contain particles a few micrometers in size would not compactly fill the narrow channels, so inks made of nanometer-sized particles were required. Physical properties of the paste, such as viscosity and yield strength, must be controlled to accommodate the filling technique that is used. The clean removal of surplus paste from the substrate is also important when the doctor blade method is used. We used a water-based paste of nano-sized silver particles to fill the 10 μm width channels, and successfully applied the developed TCF to an OSC.

The roll-to-roll imprinter was a homemade machine (TRI_-KIMM) KIMM. The flexible stamp mold was fabricated by the electroforming of nickel and cobalt alloys to a dimension of $250 \times 250\ mm^2$. A flexible mold of ~200 μm in thickness was mounted on a heating roll using two roll-click gears, as shown in Fig. 1(b). The stamp mold was a grid mesh made of rails 10 μm wide by 10 μm high with a 510 μm pitch for application to the OSC cell with an area of $10 \times 10\ mm^2$. For the substrate we used 200 μm thick thermally stabilized PEN film from DuPont-Teijin (Teonex Q65FA). The cartridge-heater in the heating roll controlled the roll temperature up to 200 °C. Fig. 1(c) shows the thermal imprinting system with a heating roll and an impression roll. The latter was coated with Cr to avoid scratching on the polymer film. The rolls with line-to-line contact could exert the maximum force of 600 kgf via a servo motor.

The imprinted micro-scale channel patterns were directly filled by the doctor blade method using the developed nano-silver paste, as shown in Fig. 1(d) and (e). This process was the same as the ink blade process used in a traditional printing method. The nano-silver paste had a silver content of >85% of the particle size, which was ~40 nm. The doctoring process was done with an acetal-polymer blade at a bevel angle of 22° and at a web speed of 15 mm/sec. Finally, as illustrated in Fig. 1(f), a

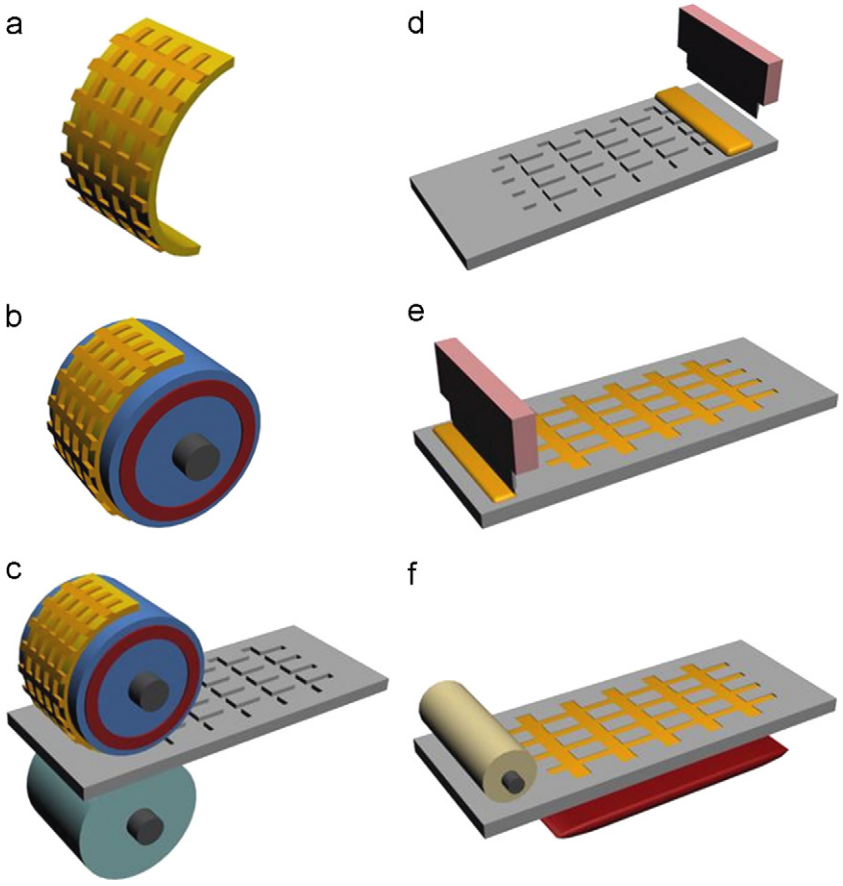

Fig. 1. Schematic diagrams of the fabrication process of Ag-embedded TCF: (a) fabrication of flexible stamp mold, (b) wrapping the stamp mold on the thermal roll, (c) roll-to-roll thermal imprinting of polymer film, (d) dropping of conductive nano-silver paste on the patterned polymer film, (e) doctor blading of nano-silver paste, and (f) roll cleaning and drying of the Ag-filled film.

roll-cleaning process was performed to remove the residue of the paste that remained on the surface of the films. The films with Ag-paste embedded in them were heat-treated at 140 °C for 2 min in a near-infrared (NIR) drying system.

The electrical resistance of the TCF was measured using a multimeter. A four-point probe system (CMT-SR1000N, AIT) was used for the resistance measurements of PEN/ poly(3,4-ethylene dioxythiophene): poly(styrene sulfonate) (PEDOT:PSS) and poly-ethylene terephthalate (PET)/ITO layers. Optical transmittance was measured using a UV–vis spectrophotometer (S-3100, SINCO). The surface roughness and topology was measured using atomic force microscopy (AFM: Asylum research-MFP 3D) and an optical microscope (OPTELICS-C130, LASERTEC).

2.2. Fabrication of ITO-free OSC devices

The purchased conductive polymer (PH1000, Heraeus) was composed of a PEDOT:PSS=1:2.5 ratio by weight showing solid contents of 1.3% and a viscosity of 50 mpa s. The polymer was mixed with 5 wt% dimethyl sulfoxide (DMSO) and 0.1 wt% fluor-osurfactant (FC-4432, 3 M) to further improve the film conductivity and the wetting of the anode film. Thus, the formulated PEDOT:PSS solution was coated by bar-coating (D-bar PO-10, OSG system) to a thickness of 100 nm followed by drying at 140 °C for 10 min on a hot plate. The solution for the photovoltaic layer was formulated by dissolving 2 wt% of a poly (3-hexylthiophene-2,5-diyl) (P3HT, Rieke Metal) and [6,6]-phenyl-C61-butyric acid methylester (PCBM, Nano-c) mixture (P3HT:PCBM=1:0.67 by weight) into 1,2-dichlorobenzene (ODCB) by stirring for 4 h at 75 °C. The solution was spin coated at 800 rpm for 30 s in a nitrogen ambient glovebox to obtain a thickness of 180 nm for the photovoltaic layer. The photovoltaic layer was solvent-annealed at room temperature for 20 min, and was then free-annealed at 130 °C for 20 min. The e-beam evaporation method was used to deposit 100 nm of aluminum at 10^{-6} Torr onto the cathode electrode, followed by a post-annealing at 140 °C for 7 min on a hot plate. The current vs. voltage characteristics was measured under solar simulation (IVT Solar) at 100 mW/cm^2 of AM 1.5 global solar illumination, which was calibrated using a standard Si photodiode.

3. Results and discussion

Fig. 2(a) shows empty channels 10 μm in width thermally imprinted on the PEN film. The imprinting force, temperature and speed must be controlled depending on the type of substrate materials and pattern shapes. In the present study, PEN film was thermally imprinted at 100 °C under 200 kgf at a speed of 15 mm/sec to the depth of the channels. Fig. 3(a) shows the AFM 3D plot and cross-sectional scans for an imprinted channel where the depth of the channel imprinted by a mold of 10 μm in height resulted in a ~3.5 μm depth. These results show that the used imprinting embedded method can fabricate channels in 10 μm width with a resolution of less than 1 μm.

The morphology of the channel filled with nano-silver paste using the doctor blade method was measured by SEM, as shown in Fig. 2(b) and (c). A clean and compact filling of the paste with clear grid edges is shown, particularly in Fig. 2(c). The excellent filling of the narrow channels and clean sheet-off from the clear PEN area was realized basically by the application of a water-based nano-sized silver paste on a hydrophobic PEN substrate. The silver particles were ~40 nm in size, which was small enough to accomplish compact packing with clean edges and boundaries, as shown in the micrometer scale drawing. The content of the solvent binder in the paste was also minimized due to the water-based properties. The paste we blended had a viscosity and yield strength that were both low relative to conventional inks, which helped with the clean filling of the channels. AFM measurement after heat treatment in the NIR dry system revealed a depth of ~1 μm in the channels (Fig. 3(b)) indicating a shrink and evaporation of the embedded paste during the heat treatment. When a different kind of paste (a solvent-based paste) was used, the doctor blade method neither completely filled the channels nor cleanly removed the residue from the PEN substrate, as shown in Fig. 2(d). A non-optimized water-based paste also

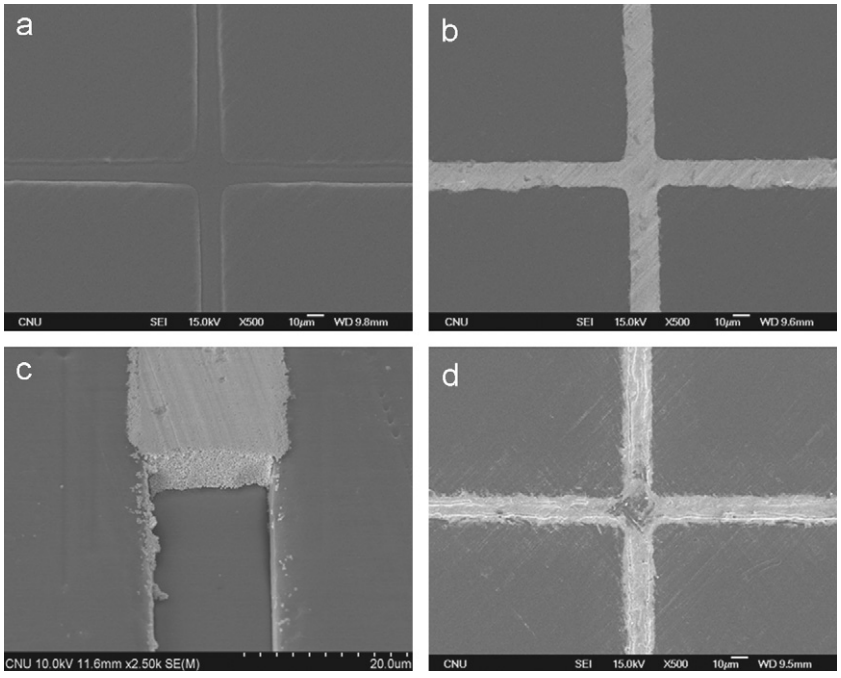

Fig. 2. SEM images of (a) a roll-to-roll imprinted grid pattern on PEN film, (b) a pattern on PEN film filled with water-based nano-silver paste, (c) a cross-sectional view of the Ag-filled channel, and (d) a pattern filled with solvent-based nano-silver paste showing residue after doctor blading.

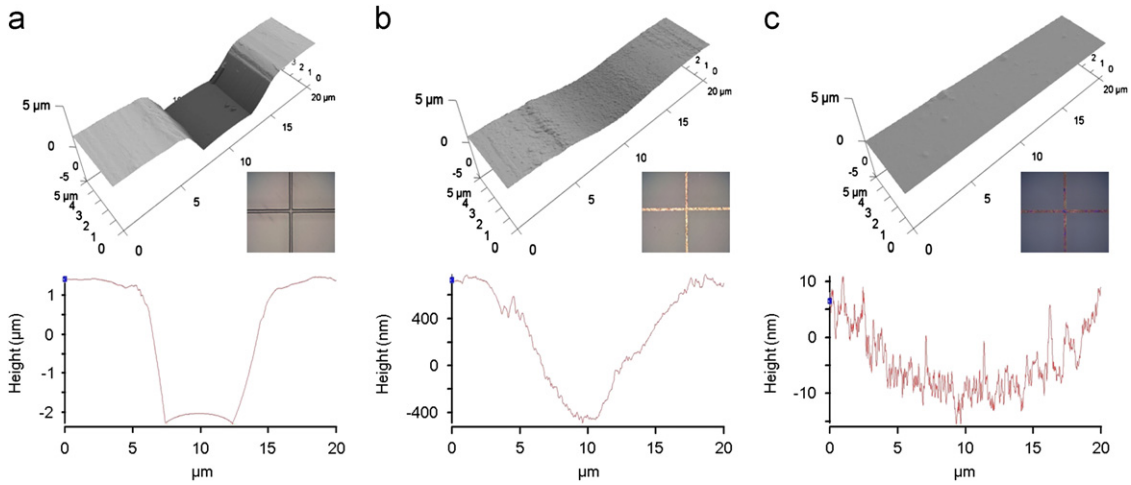

Fig. 3. AFM and optical microscope image of (a) a roll-to-roll imprinted pattern on PEN film, (b) a pattern filled with nano-silver paste and heat treated, and (c) a pattern paste filled followed by coating with PEDOT:PSS.

showed an incomplete filling of the channels (not shown). The comparison clearly reveals the importance of controlling the physical properties of the paste to fill such narrow grid channels. Note also that the developed water-based nano-silver paste is environment friendly.

The process for embedding metal grids requires the additional step of channel fabrication in addition to the printing step, but the reward was a reduced roughness in the device films fabricated for the TCF. The conducting polymer for application to OSCs has typically been PEDOT: PSS.[14] Fig. 3(c) shows a AFM 3D plot and the cross-sectional scans for the PEDOT:PSS film coated on the paste-filled channel shown in Fig. 3(b). The surface roughness measured ~20 nm, which led us to expect uniform film thicknesses in the devices. This is one of the reasons to use an embedded channel with TCFs, and the other aspects will be discussed later relative to OSC application.

Optical transmittance and electrical conductance are the major objectives of TCFs. The properties of the fabricated TCF electrode embedded with nano-silver paste (sample PEN/Ag-mesh) were measured. The properties were also compared with those of ITO-deposited PET film (sample PET/ITO) and PEDOT:PSS-coated PEN film (sample PEN/PEDOT:PSS). For the PET/ITO sample, ITO film was deposited onto PET film (180 μm thickness) by sputtering ITO to a thickness of 160 nm, and for the PEN/PEDOT:PSS sample, 100 nm thick PEDOT:PSS film was coated using a bar coater. The optical transmittance of these samples was measured at various wavelengths, and is summarized in Fig. 4. A reference measurement of transmittance for bare PEN film showed an 85% at 550 nm and slightly increased with increase in wavelength. The PET/ITO showed the lowest performance particularly with respect to a large transmission loss in the small and large wavelength regions. PEN/PEDOT:PSS film showed a decreasing transmittance at >600 nm. The transmittance of PEN/Ag-mesh film followed that of the bare PEN film with values that were ~4% less. The same level of transmittance loss was noticeable through all wavelength regions, and the loss could be accounted for by the exact amount of light blocking with the grid line area.

Table 1 summarizes the sheet resistance, optical transmittance at 550 nm, and σ_{DC}/σ_{OP} of the above films. The sheet resistance of the PEN/Ag-mesh film was measured using a formula reported by Hautcoeur et al [15]. The electrical-to-optical conductance ratio, σ_{DC}/σ_{OP}, has been taken as a figure-of-merit of TCFs [16,17], and is particularly useful in comparing the performance of films with differing values for electrical resistance and optical transmittance. The exceptionally higher ratio value of 237 for the PEN/Ag-mesh

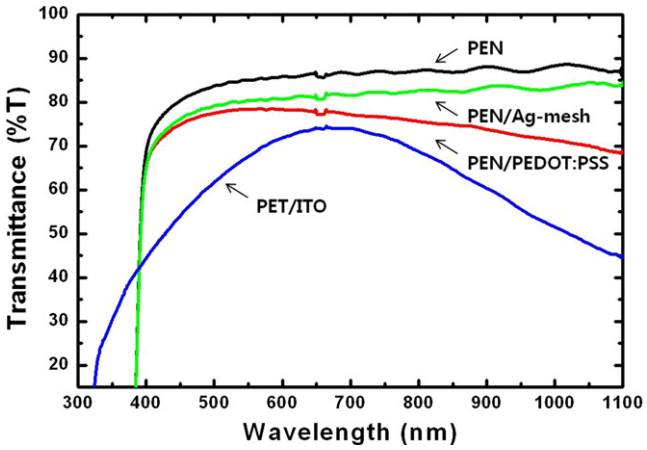

Fig. 4. Optical transmittance measured with varying wavelengths 300–1100 nm for PEN film,100 nm thick PEDOT:PSS coated PEN film, roll-to-roll imprinted PEN film with embedded Ag-mesh, ITO coated PET film.

film (more than 58 for PET/ITO and 16 for PEN/PEDOT:PSS) clearly indicates the advantage of the grid-type films over other thin films like PET/ITO. This result can be expected from films with the highest optical transmittance even with the lowest resistance among the samples. Another characteristic of grid-type TCFs is that the absorption of a characteristic wavelength with a particular type of thin film can be avoided. As noted above, the transmittance and conductance of TCFs is determined only by the pitch of the mesh pattern and the width and depth of the channel, respectively.

To check the applicability of the developed PEN/Ag-mesh film to the electrode of an OSC, we fabricated a simple OSC. Other TCFs (PET/ITO and PEN/PEDOT: PSS) were also fabricated for OSCs for the purpose of comparison. The hole transport layer (HTL), active layer, and Al cathode were sequentially deposited onto the anode TCFs. ITO film, 160 nm in thickness, was patterned by laser scribing. Highly conductive PEDOT:PSS was used for the HTL, and a blend of P3HT:PCBM was used for the active bulk heterojunction layer. The processing details are described in Section 2. The fabricated flexible OSCs had an active area of 10×10 mm^2, and were analyzed with a solar simulator, as summarized in Fig. 5 and Table 2. The schematic of the OSC structure is shown in the inset of Fig. 5. Also shown by the inset is the bent OSC. The bent

Table 1
Sheet resistance, transmittance and σ_{DC}/σ_{OP} characteristics of PET/ITO, PEN/PEDOT:PSS, and PEN/Ag-mesh substrate films.

Substrates	Sheet resistance (Ω/□)	Transmittance (% at 550 nm)	σ_{DC}/σ_{OP}
PET/ITO	14.89	67.61	58.40
PEN/PEDOT:PSS	90.42	78.33	16.00
PEN/Ag-mesh	6.85	80.35	237.42

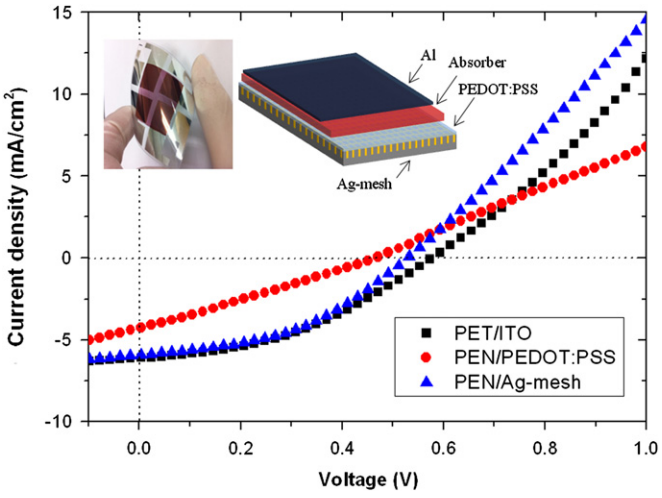

Fig. 5. Current density versus voltage characteristics of the OSCs fabricated using the roll-to-roll imprinted PEN/Ag-mesh film, bar-coated PEN/PEDOT:PSS film, and PET/ITO film. Inset shows the fabricated flexible OSC and its schematic structure.

Table 2
Organic solar cell performance of roll-to-roll imprinted TCF (PEN/Ag-mesh) cell, PEN/PEDOT:PSS cell and low-resistance PET/ITO cell.

Substrate	V_{oc} (V)	J_{sc} (mA/cm^2)	FF	PCE(%)
PET/ITO	0.61	6.20	0.45	1.70
PEN/PEDOT:PSS	0.38	3.63	0.25	0.35
PEN/Ag-mesh	0.57	6.10	0.39	1.40

electrode revealed no resistivity changes suggesting the stability of the embedded grids, but a systematic examination of the bending effect is necessary.

The OSC fabricated on PEN/PEDOT:PSS anode film showed a relatively poor performance with a 0.35% power conversion efficiency (PCE). The high series resistance of PEDOT:PSS film when used as the electrode (without a main high-conductance electrode) could lead to a smaller open circuit voltage (V_{oc}) and could degrade the current-collecting efficiency with a smaller short circuit current density (J_{sc}) and fill factor (FF). When the Ag-mesh electrode is inserted below the PEDOT:PSS anode film (or PEN/Ag-mesh electrode), V_{oc}, J_{sc}, FF and PCE improved to 0.57 V, 6.10 mA/cm^2, 0.39, and 1.40%, respectively. This was because the high conductance Ag-mesh anode efficiently collected the current. The J_{sc} value was similar to that for a PET/ITO anode film, but all the parameters showed slightly lower values resulting in a lower PCE (1.40%) compared with that of a PET/ITO-made OSC (1.70%). The smaller work function of Ag (4.2 eV), compared with that of ITO (4.7 eV), could have affected the current flow from PEDOT:PSS [18] and led to a reduced V_{oc} and FF, and consequently a reduced PCE. Further enhancement of OSC performance may be achieved via optimization of layer thicknesses and doping [19], band engineering of the layers [20], and process controls [21], etc. As such, while the optimization of the TCF application to an OSC is a task that remains to be accomplished, we demonstrated that a large-area, flexible TCF of embedded metal grids can successfully be used for organic solar cell devices with a performance that approaches that of conventional ITO-based OSCs.

4. Conclusions

We fabricated a flexible large-area TCF with embedded silver grids via the development of a roll-to-roll thermal-imprinting process combined with a doctor blade method. We fabricated a fine-line channel that was 10 μm in width on a PEN substrate via thermal imprinting, an accomplishment that is difficult when using conventional roll-to-roll processing. The physical properties of the paste were controlled in order to completely fill the narrow channels. The paste was basically composed of nano-size silver particles dispersed in water. Doctor blading of the paste was used to fill the channels compactly and to cleanly remove the residue from the PEN substrate. The PEN substrate was embedded with silver grids and revealed excellent electrical and optical performances as transparent conductive film with an extremely high σ_{DC}/σ_{OP} value of 237. This roll-to-roll printable TCF was also successively connected to another roll-to-roll-based printing technique for organic solar cell fabrication. An OSC with a PCE of 1.40%, unoptimized but approaching that of an ITO-based OSC (1.70%), was demonstrated with the successful application of the developed flexible TCF. A reasonable OSC performance was facilitated partly by improving the topology (with engraving roughness of ~20 nm) and reducing the shadowing loss (with 10 μm -width fine-line grids).

Acknowledgment

This study was supported by a grant (20103060010010) funded by the Korea institute of Energy Technolgy Evaluation and Planning ("KETEP") and a grant (B551179-08-03-00) funded by the Korea Research Council Industrial Science and Technology, Republic of Korea. One of the authors (DJK) was supported by the NRL program of the National Research Foundation, Republic of Korea.

References

[1] W. Gaynor, G.F. Burkhard, M.D. McGehee, P. Peumans, Smooth nanowire/polymer composite transparent electrodes, Advanced Materials 12 (2011) 2905–2910.
[2] Y.H. Kim, C. Sachse, M. Machala, C. May, L.M. Meskamp, K. Leo, Highly conductive PEDOT:PSS electrode with optimized solvent and thermal post-treatment for ITO-free organic solar cells, Advanced Functional Materials 21 (2011) 1076–1081.
[3] P. Roberto, M. Rebeca, P.G. Cristina, J.A. Pomposo., G. Hans, A. Javier, M. David, Combined electrochromic and plasmonic optical responses in conducting polymer/metal nanoparticle films, Journal of Nanoscience and Nanotechnology 7 (2007) 2938–2941.
[4] M.W. Rowell, M.A. Topinka, M.D. McGehee, H.J. Prall, G. Dennler, N.S. Sariciftci, L. Hu, G. Gruner, Organic solar cells with carbon nanotube network electrodes, Applied Physics Letters 88 (2006) 233506.
[5] G. Eda, Y.Y. Lin, S. Miller, C.W. Chen, W.F. Su, M. Chhowalla, Transparent and conducting electrodes for organic electronics from reduced grapheme oxide, Applied Physics Letters 92 (2008) 233305.
[6] J.Y. Lee, S.T. Connor, Y. Cui, P. Peumans, Solution-processed metal nanowire mesh transparent electrodes, Nano Letters 8 (2008) 689–692.
[7] C.H. Liu, X. Yu, Silver nanowire-based transparent, flexible, and conductive thin film, Nanoscale Research Letters 6 (2011) 75–82.
[8] Y. Zhou, H. Cheun, S. Choi, W.J. Potscavage, F. Hernandez, Indium tin oxide-free and metal-free semitransparent organic solar cells, Applied Physics Letters 97 (2010) 153304.
[9] M.G. Kang, M.S. Kim, J. Kim, L.J. Guo, Organic solar cells using nanoimprinted transparent metal electrodes, Advanced Materials 20 (2008) 4408–4413.

[10] K. Tvingstedt, O. Inganas, Electrode grids for ITO-free organic photovoltaic devices, Advanced Materials 19 (2007) 2893–2897.
[11] Y. Galagan, J.M. Rubingh, R. Andriessen, C. Fan, P.M. Blom, S. Veenstra, J. Kroon, ITO-free flexible organic solar cells with printed current collecting grids, Solar Energy Materials and Solar Cells 95 (2011) 1339–1343.
[12] R. Sondergaard, M. Hosel, D. Angmo, T.T. Larsen-Olsen, F.C. Krebs, Roll-to-roll fabrication of polymer solar cells, Materials Today 15 (2012) 36–49.
[13] H. Becker, U. Heim, Hot embossing as a method for the fabrication of polymer high aspect ratio structures, Sensors and Actuators 83 (2000) 130–135.
[14] S.I. Na, S.S. Kim, J. Jo, D.Y. Kim, Efficient and flexible ITO-free organic solar cells using highly conductive polymer anodes, Advanced Materials 20 (2008) 4061–4067.
[15] J. Hautcoeur, X. Castel, F. Colomber, R. Benzerga, M. Himdi, G. Legeay, E. Motta, Transparency and electrical properties of meshed metal films, Thin Solid Films. 519 (2011) 3851–3858.
[16] S. De, T.M. Higgins, P.E. Lyons, E.M. Doherty, P.N. Nirmalraj, W.J. Blau, J.J. Boland, J.N. Coleman, Silver nanowire networks as flexible, transparent, conducting films: extremely high DC to optical conductivity ratios, ACS Nano 3 (2009) 1767–1774.
[17] L. Hu, H. Wu, Y. Cui, Metal nanogrids, nanowires, and nanofibers for transparent electrodes, MRS Bulletin 36 (2011) 760–765.
[18] M.R. Lilliedal, in Roll-to-Roll Processing of Polymer Solar Cells, Master Thesis, Riso DTU, Denmark, Chapter 4, 2010.
[19] A.J. Moule, J.B. Bonekamp, K. Meerholz, The effect of active layer thickness and composition on the performance of bulk-heterojunction solar cells, Journal of Applied Physics 100 (2006) 094503.
[20] L.S. Hung, C.W. Tang, M.G. Mason, Enhanced electron injection in organic electroluminescence devices using an Al/LiF electrode, Applied Physics Letters 70 (1997) 152–154.
[21] C. Zhang, S.W. Tong, C. Zhu, C. Jiang, E.T. Kang, Enhancement in open circuit voltage induced by deep interface hole traps in polymer-fullerene bulk heterojunction solar cells, Applied Physics Letters 94 (2009) 103305.